Q. J. R. Meteorol. Soc. (1997), **123**, pp. 2477–2498

An explicit flux-form semi-Lagrangian shallow-water model on the sphere

By SHIAN-JIANN LIN[1]* and RICHARD B. ROOD[2]

[1]*Goddard Space Flight Center and University of Maryland Baltimore County, USA*
[2]*Goddard Space Flight Center, USA*

(Received 20 June 1996; revised 22 November 1996)

SUMMARY

A global shallow-water model based on the flux-form semi-Lagrangian scheme is described. The mass-conserving flux-form semi-Lagrangian scheme is a multidimensional semi-Lagrangian extension of the higher order Godunov-type finite-volume schemes (e.g., the piece-wise parabolic method). Unlike the piece-wise parabolic methodology, neither directional splitting nor a Riemann solver is involved. A reverse engineering procedure is introduced to achieve the goal of consistent transport of the absolute vorticity and the mass, and hence, the potential vorticity. Gravity waves are treated explicitly, in a manner that is consistent with the forward-in-time flux-form semi-Lagrangian transport scheme. Due to the finite-volume nature of the flux-form semi-Lagrangian scheme and the application of the monotonicity constraint, which can be regarded as a subgrid-scale flux parametrization, essentially noise-free solutions are obtained without additional diffusion. Two selected shallow-water test cases proposed by Williamson *et al.* (1992) and a stratospheric vortex erosion simulation are presented. Discussions on the accuracy and computational efficiency are given based on the comparisons with a Eulerian spectral model and two advective-form semi-implicit semi-Lagrangian models.

KEYWORDS: Computational test cases Conservative advection Numerical techniques

1. INTRODUCTION

Numerical approximations to the intrinsically nonlinear advection process are a difficult and important part of modelling a complete fluid dynamical system. Modern advection algorithms such as the van Leer-type schemes (van Leer 1974, 1977, and 1979; Lin *et al.* 1994), Multidimensional Flux-Corrected Transport (MFCT) (Zalesak 1979), Total Variationally Diminishing schemes (TVD) (Harten 1983), Piece-wise Parabolic Method (PPM) (Colella and Woodward 1984), the advective-form semi-Lagrangian schemes (reviewed by Staniforth and Côté 1991), and the Flux-Form Semi-Lagrangian (FFSL) scheme (Lin and Rood 1996), are increasingly being used in geophysical fluid dynamics applications. Most of these schemes are either monotonicity-preserving by design or can be made monotonic (shape preserving) with an additional constraint (Williamson and Rasch 1989). Much of the motivation has been to improve the accuracy and physical basis of the constituent advection. In choosing an optimal advection scheme for a particular fluid dynamics problem, not only does the scientific merit of an algorithm need to be considered, but also its suitability to the computational platform.

Traditionally, the two most widely used algorithms for numerical weather predictions and climate simulations are the spectral transform method (e.g., Bourke 1972) and the centred finite-differencing method (e.g., Arakawa and Lamb 1981). Motivated by better computational efficiency, semi-implicit semi-Lagrangian methods are widely used with both spectral and grid-point approaches (e.g., Tanguay *et al.* 1990; Bates *et al.* 1993; Williamson and Olson 1994; Ritchie *et al.* 1995). Beyond better computational efficiency, the improved accuracy due to the semi-Lagrangian advection has also been shown to impact positively on model performance. For instance, Rasch and Williamson (1991) have shown large changes in model climatology by replacing only the water vapour transport equation in a traditional spectral model (the NCAR Community Climate Model) with a more physically based semi-Lagrangian algorithm. For long-term climate simulations,

* Corresponding author: Data Assimilation Office, Laboratory for Atmospheres, NASA/Goddard Space Flight Center, Greenbelt, MD 20771, USA. e-mail: lin@dao.gsfc.nasa.gov.

however, there remain legitimate concerns about the non-conservative nature of many of the semi-Lagrangian algorithms currently in use.

Monotonicity-preserving finite-volume schemes (e.g., the higher order Godunov-type methods by van Leer and the PPM), although widely used in engineering and astrophysics, have not been widely adopted in meteorological or oceanographic researches. Carpenter *et al.* (1990), Allen *et al.* (1991), Thuburn (1993), and Lin *et al.* (1994) are among the first to apply such schemes to meteorological problems. These finite-volume schemes are mass-conserving and fundamentally one-dimensional (1-D). Normally, to apply them in multidimensional situations operator splitting is used. An error proportional to the size of the time-step (Δt) exists in split approaches to multidimensional problems, which is perhaps the major reason these schemes are not widely used in meteorology and oceanography. To reduce the splitting error and also to enhance the computational efficiency, Lin and Rood (1996, LR hereafter) developed the Flux-Form Semi-Lagrangian (FFSL) scheme, which is a multidimensional and semi-Lagrangian extension of the above mentioned 1-D finite-volume schemes. Due to its flux-form construction, conservation of the mass is automatic. The finite-volume discretization is local, which not only has an advantage for modelling flows with sharp gradients, but also makes it more suitable (as compared with, for example, the spectral method) in a distributed computing environment using the domain decomposition technique. Our main objective here is to apply the FFSL scheme, a transport scheme initially developed for passive scalars, to hydrostatic geophysical flows. The purpose is to evaluate the impact of physically based advection algorithms on the complete equations of large-scale geophysical flow.

For general non-hydrostatic flows, Godunov-type finite-volume algorithms require a Riemann solver, which is usually formulated as a 1-D problem. Multidimensionality is achieved via the sequential operator splitting (see for example, Carpenter *et al.* 1990). The Riemann solver is needed to represent discontinuities or shock waves, which are the rule rather than the exception in aerodynamic or astrophysical applications (e.g. Woodward and Colella 1984). Hydrostatic geophysical flows, on the other hand, are dominated by smoothly varying large-scale motions, which is particularly true from a global perspective (e.g., in climate simulations or medium-range weather forecasts). To the best of our knowledge, a multidimensional Riemann solver has not yet been developed for hydrostatic primitive equations. Even if such a solver can be developed, its complexity will be likely to render the whole model computationally inefficient, as compared with established methods, for geophysical flows. One could possibly use the 1-D Riemann solver in a sequential fashion, but this would defeat the purpose of a multidimensional transport scheme, which is far superior to its operator-split counterpart. In the light of this consideration, we avoid tackling a very difficult multidimensional Riemann problem and choose instead a more conventional approach for computing the pressure gradient terms and the 'time-averaged advective winds' (see sections 2 and 3 for definition).

We propose here an algorithm for applying the FFSL transport scheme to a complete dynamical framework, the shallow-water equations. The shallow-water system of equations is nearly equivalent to the system governing the inviscid compressible flow equations (i.e. the Euler equations) in two-dimensions. It also represents the horizontal dynamics of the 3-D hydrostatic primitive-equation system and is therefore often the first step in developing numerical weather prediction and general circulation models. The FFSL transport scheme will be applied directly to the conservation law for the 'mass', and indirectly to the conservation law for the 'absolute vorticity', via a reverse-engineering procedure with a two-grid system (a combination of the C- and D-grid; see section 3), which has the advantage of the Z-grid (Randall; 1994), but without the need to invert vorticity and divergence.

In section 2 we will briefly review the multidimensisonal FFSL algorithm. The philosophy and details of the discretization of the shallow-water equation set will be given in section 3. Particular attention will be placed on the consistent transport of the 'mass' and the 'absolute vorticity' (and therefore, the potential vorticity) by the chosen transport scheme using the vector-invariant form of the equations. In section 4, two of the reference tests proposed by Williamson *et al.* (1992) will be performed to evaluate the proposed algorithm. In addition a stratospheric vortex erosion problem will be presented. Finally, a discussion and summary is provided.

2. The multidimensisonal FFSL scheme on the sphere—a brief review

The multidimensional FFSL scheme is derived from a direction-split perspective using strictly 1-D operators. A procedure is then applied to remove the directional bias and the dominant (first-order) error resulting from the splitting approach. We will only highlight the development of the 2-D FFSL transport scheme. Detailed derivation, as well as error and stability analyses, are given in LR. The conservation law (the transport equation) for a density-like field Q (e.g., in the context of the shallow-water equations, Q may represent the depth of the fluid and/or the absolute vorticity) is

$$\frac{\partial}{\partial t} Q + \nabla \cdot (\mathbf{V} Q) = 0 \tag{1}$$

where $\mathbf{V} = (u, v)$ is the horizontal vector velocity and t represents the time dimension. To model Eq. (1), we define F and G as the 1-D flux-form operators for updating Q for one time-step in the zonal (λ) and meridional (θ) directions, respectively. The 1-D operators are assumed only to be 1-D finite-volume scheme, but no explicit form of the 1-D operator is assumed a priori. Adopting the following standard difference δ and average $\overline{()}$ notations,

$$\delta_\sigma q = q\left(\sigma + \frac{\Delta\sigma}{2}\right) - q\left(\sigma - \frac{\Delta\sigma}{2}\right) \tag{2}$$

$$\overline{q}^{\sigma} = \frac{1}{2}\left[q\left(\sigma + \frac{\Delta\sigma}{2}\right) + q\left(\sigma - \frac{\Delta\sigma}{2}\right)\right]. \tag{3}$$

F and G can be written as follows:

$$F(u^*, \Delta t; Q^n) = -\frac{\Delta t}{A\Delta\lambda \cos\theta}\delta_\lambda \left[\mathscr{X}(u^*, \Delta t; Q^n)\right] \tag{4}$$

$$G(v^*, \Delta t; Q^n) = -\frac{\Delta t}{A\Delta\theta \cos\theta}\delta_\theta \left[\cos\theta \mathscr{Y}(v^*, \Delta t; Q^n)\right] \tag{5}$$

where A is the radius of the sphere, λ the longitude, and θ the latitude. $\mathscr{X}$ and $\mathscr{Y}$, the time-averaged fluxes of Q in the zonal and meridional direction, respectively, are defined as

$$\mathscr{X}(u^*, \Delta t; Q^n) = \frac{1}{\Delta t}\int_t^{t+\Delta t} uQ \, dt - \text{hot} \tag{6}$$

$$\mathscr{Y}(v^*, \Delta t; Q^n) = \frac{1}{\Delta t}\int_t^{t+\Delta t} vQ \, dt - \text{hot} \tag{7}$$

where 'hot' stands for the 'higher order terms'. To approximate the 'time-averaged flux' $\mathscr{X}$ (or $\mathscr{Y}$) across the boundaries of the grid cell (see Fig. 1), properly defined time-averaged (or

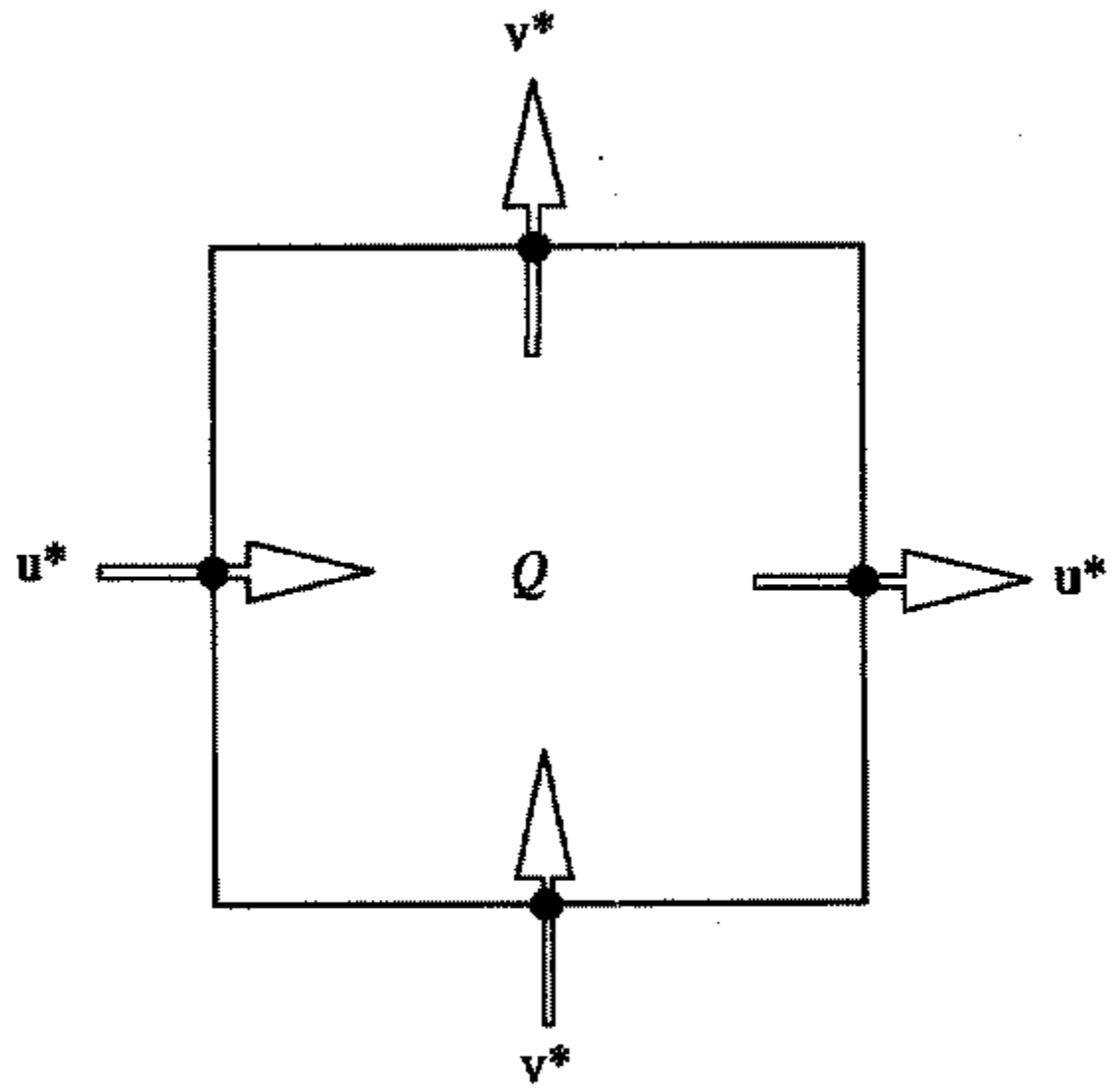

Figure 1. Schematics of the 'C-grid' arrangement for the transport of the cell-averaged density-like Q field by the 2-D FFSL scheme.

time-centred) winds, (u^*, v^*), and the cell-averaged field at time-level n, Q^n, are required. The fluxes are then used for updating the cell-averaged fields to the next time-level. As illustrated in Fig. 1, the advective winds and the cell-averaged Q field (the 'mass') are defined on the C-grid (see Mesinger and Arakawa 1976 for the definition of grids A–E). For convenience in the presentation, we will omit, in the rest of this section, the dependence of the F and G operators on (u^*, v^*) and Δt.

Cross-derivative terms which are essential to a scheme's stability in multidimensions are automatically included by applying the 1-D operators sequentially. However, the sequential splitting process introduces a 'splitting error' term, which is usually directionally asymmetric. The first step to achieving the desired multidimensionality is to remove directional biases by averaging two anti-symmetric operator-split algorithms (F followed by G, or G followed by F; see section 2 in LR). The resulting directional-bias free algorithm is

$$Q^{n+1} = Q^n + F[Q^n + \tfrac{1}{2}G(Q^n)] + G[Q^n + \tfrac{1}{2}F(Q^n)]. \tag{8}$$

Scheme (8) still suffers from the 'deformational error'. Smolarkiewicz (1982) demonstrated this type of error using the Crowley scheme in a deformational flow field. An immediate consequence of this error is that a constant Q field will not remain constant in a non-divergent flow. Furthermore, it can be verified that linear correlation between constituents will not be preserved by the above algorithm. To address these problems, the second step is to replace F and G inside the square brackets in (8), the contributions from the cross-stream directions, with their *advective-form* counterparts f and g, respectively, to arrive at the following form of the 2-D FFSL scheme.

$$Q^{n+1} = Q^n + F[Q^n + \tfrac{1}{2}g(v_a^*, \Delta t; Q^n)] + G(Q^n + \tfrac{1}{2}f(u_a^*, \Delta t; Q^n)] \tag{9}$$

where

$$u_a^* = \overline{u^*}^{\lambda}, \; v_a^* = \overline{v^*}^{\theta}.$$

Scheme (9) is free of the deformational error and preserves linear constituent correlation exactly, even when a monotonicity constraint is enforced (see LR for the proof). In

the context of the shallow-water system, transport of the fluid depth (h) and the absolute vorticity (Ω) by scheme (9) ensures that h and Ω are better correlated during the time-marching, which in turn ensures that the potential vorticity ($\mathrm{PV} = \Omega/h$), a very important dynamical quantity, is better simulated (see section 4).

The generalization of scheme (9) to large time-step (Courant number greater than one), which only involves slight modification to the 1-D operators, is described in LR. Equation (9) will be used in the next section to discretize the transport equations for the 'mass' (h) and the 'absolute vorticity' (Ω) in the shallow-water system of equations.

3. Discretization of the shallow-water equations with the 2-D FFSL scheme

The mass conservation law for a shallow layer of 'water', which in effect can be any Newtonian fluid, is

$$\frac{\partial}{\partial t}h + \nabla \cdot (\mathbf{V}h) = 0 \tag{10}$$

where h represents the depth of the fluid (the 'mass' in the shallow-water system). The vector-invariant form of the momentum equation in spherical coordinates can be written concisely in component form as follows:

$$\frac{\partial}{\partial t}u = \Omega v - \frac{1}{A\cos\theta}\frac{\partial}{\partial \lambda}[\kappa + \Phi] \tag{11}$$

$$\frac{\partial}{\partial t}v = -\Omega u - \frac{1}{A}\frac{\partial}{\partial \theta}[\kappa + \Phi] \tag{12}$$

where A = radius of the earth, λ = longitude, θ = latitude, $\Phi = \Phi_s + gh$, the free surface geopotential (g is the gravitational acceleration), Φ_s = the surface geopotential, $\Omega = 2\omega \sin\theta + \nabla \times \mathbf{V}$, the absolute vorticity, ω = angular velocity of the earth, and $\kappa = \frac{1}{2}\mathbf{V} \cdot \mathbf{V}$, the kinetic energy.

Equations (10), (11) and (12) form a complete set of equations. A significant advantage of the vector invariant form of the momentum equation is that the metric terms, which are singular at the poles, are absorbed into the definition of the relative vorticity, which is well defined (i.e., non-singular) at the poles. (The relative vorticity at the poles can be computed non-singularly by the *Stokes' theorem* (see Eq. (19)).) A disadvantage of this form is that the discretized form of the kinetic energy κ needs to be formulated carefully to minimize inconsistency between $\nabla\kappa$ and the (discretized) absolute vorticity fluxes ($u\Omega$ and $v\Omega$). This inconsistency manifests itself as a spurious momentum source and could result in the 'Hollingsworth–Kållberg instability' (Hollingsworth *et al.* 1983; Suarez and Takacs 1995).

The vector-invariant form of the equations can be easily converted to the (scalar) vorticity–divergence form. The conservation law for the absolute vorticity can be readily obtained by taking curl of the vector momentum equation [i.e., $\nabla \times$ (11, 12)]

$$\frac{\partial}{\partial t}\Omega + \nabla \cdot (\mathbf{V}\Omega) = 0. \tag{13}$$

The divergence ($\eta = \nabla \cdot \mathbf{V}$) equation is obtained by applying the divergence operator to the same vector equation. If the vorticity–divergence form is discretized, a way must be found to invert the pair (Ω, η) back to (u, v) each time-step for the time integration to proceed. The spectral transform method (e.g., Bourke 1972) is ideally suited to this purpose because

the inversion is nearly trivial. Models based on a local discretization method (e.g., finite-difference or finite-volume schemes) would need to solve an elliptic equation, which may in some cases be nonlinear and inefficient to solve (e.g., Bates *et al.* 1995, B95 hereafter).

Due to the continuous differentiability of the basis functions used in the spectral transform method, there appears to be no theoretical advantage for the spectral method to choose the vorticity–divergence form over the usual, or vector-invariant, form of the momentum equations. In fact, they are equivalent for the spectral method if the algorithm is designed properly (Ritchie *et al.* 1995).

There are, however, significant advantages in choosing the vorticity–divergence form when local discretization methods are used. Within the linearized shallow-water equations framework, Randall (1994) discussed in detail the superior wave-dispersion property associated with the vorticity–divergence form (the 'Z-grid'). For the nonlinear processes, a less publicized yet important advantage of the vorticity–divergence form is that the transport of the (absolute or relative) vorticity, a higher-order conservative scalar, is modelled directly. To retain these advantages while avoiding solving an elliptic equation, the idea introduced by Sadourny (1975) and Arakawa and Lamb (1981, AL hereafter) can be generalized to discretize the vector-invariant form of the momentum equations. AL's method amounts to a subtle second-order centre-in-space differencing to (10), (11), and (12) on the C-grid. Some design constraints are enforced to ensure that, after taking curl of the centre-differenced form of (11) and (12), the resulting vorticity equation is reduced to the celebrated 'Arakawa Jacobian' for vorticity advection (Arakawa 1966) when the flow is non-divergent. To avoid the Hollingsworth–Kållberg instability, the numerical form of the kinetic energy κ, particularly near the poles, needs to be carefully constructed (Suarez and Takacs 1995). AL's method, as well as the spectral method, is a spatial discretization technique. Temporal discretization is independently treated, usually by a leapfrog scheme. In the proposed algorithm using the FFSL transport scheme, spatial and temporal discretizations are intrinsically non-separable (for the nonlinear transport processes), which, mathematically speaking, results in a beneficial cancellation between the spatial and temporal truncation errors. Physically, the FFSL scheme emulates the entire transport process based on the fundamental control-volume concept.

A design feature of AL's method is that, in the absence of time discretization error, both the total energy and potential enstrophy are conserved in the point-wise sense. A subgrid-scale mixing parameterization must be specified for simulating realistic flows. In reality, the total energy and enstrophy will not and should not be conserved after the subgrid-scale mixing process is involved or, equivalently, if the discretized variables are to be considered as *cell-averaged* values.

The FFSL algorithm is designed to model the cell-averaged variables, and hence will only conserve 'mass' (depth of the fluid h) and the h-weighted potential vorticity, the absolute vorticity. Energy and potential enstrophy will, in general, decrease monotonically in time due to the subgrid mixing algorithm implicitly chosen with monotonic 1-D finite-volume flux-form operators. This should be contrasted with commonly used subgrid mixing processes such as the Shapiro filter (Shapiro 1970), harmonic diffusion, and Smagorinsky's nonlinear diffusion (Smagorinsky *et al.* 1965). The physical basis and interpretation of these subgrid mixing processes varies widely.

When the van Leer or the PPM schemes are chosen an implied subgrid distribution is also chosen. This distribution is piece-wise linear for the van Leer scheme and piece-wise parabolic with the PPM. When a monotonicity constraint is applied local extrema are prohibited by re-adjusting the subgrid distribution. This adjustment process emulates the local mixing mechanisms. Since parabolic distributions allow more structure than the linear distributions, PPM schemes are generally less diffusive than van Leer schemes. In

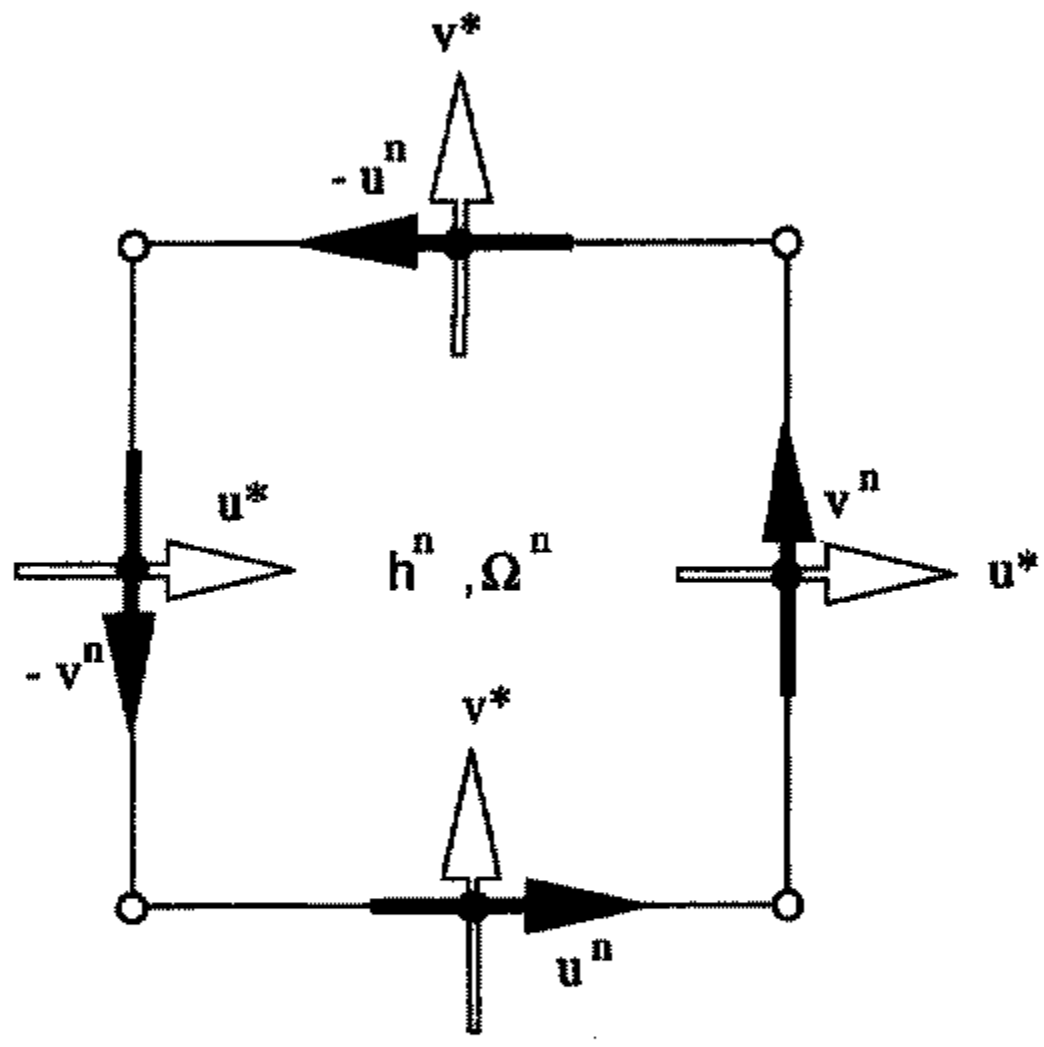

Figure 2. Schematics of the two-grid system: the 'CD-grid'. The time-centered advective winds (u^*, v^*) (the hollow arrows) are staggered as in the C-grid (as in Fig. 1) whereas the prognostic winds (u^n, v^n) (the solid arrows) are staggered as in the D-grid. The cell-averaged relative vorticity is computed by the Stokes theorem.

both cases, however, the diffusion is scale-dependent and nonlinear. As argued in Rood *et al.* (1992), there is some evidence that the nonlinear diffusion associated with monotonic advection schemes can be interpreted physically, at least for stratospheric tracer problems. Consequently, in the current implementation of the FFSL algorithm for solving the shallow-water equations no explicit diffusion will be needed.

Another important difference between the FFSL algorithm and AL's method is in the way absolute vorticity is transported in a general divergent flow. In the current approach the discretized h and Ω fields are taken as cell-averaged values, not point-wise values, and the same scheme is used for transporting h and Ω, regardless of the divergence of the flow. Functional relations between h and Ω can therefore be better preserved. In AL's approach, the equation for the fluid depth h (Eq. (10)) is centre-differenced in a straightforward manner while (11) and (12) are centre-differenced, in a more sophisticated way, to achieve the goal of vorticity transport by the Arakawa Jacobian for non-divergent flow. Therefore, the transport scheme for h and Ω in AL's approach will be, in general, different. As a consequence, an initial linear and/or nonlinear functional relationship between these two conservative variables will be lost during the course of time integration. Therefore, the AL approach does not maintain the analytic relationships which are derived from basic physical principles.

To achieve the goal of transporting h and Ω by exactly the same manner, an obvious requirement is that h and Ω be defined at the same point (or, in the finite-volume sense, enclosed in the same cell). Since our prognostic variables are h and (u, v), rather than h and (Ω, η), the D-grid arrangement (see Fig. 2) is the logical choice. As tangential winds are defined along the cell boundaries, the D-grid is ideally suited for computing the circulation (and hence, the *cell-averaged* relative vorticity, in the *mean value theorem* sense). It is also the best grid on which to compute geostrophically balanced flow. It is known that any single-grid system, other than the C-grid or the Z-grid (Randall 1994), generates two-grid-length gravity waves. This problem can be avoided by computing the time-centred advective winds (u^*, v^*) on the C-grid, as required by the multidimensional FFSL scheme

(see Fig. 1). We shall consider (u^*, v^*) on the C-grid as given and defer discussion on how they should be computed after the discretization of the governing equations on the D-grid is presented.

It is observed that if the first term on the right hand side (r.h.s.) of (11) and (12) is interpreted as the time-averaged (from time t to time $t + \Delta t$) meridional and zonal flux of the absolute vorticity (see the definition in (6) and (7), respectively, a consistently discretized absolute vorticity equation can be formed by taking the curl, numerically, of these two discretized component equations. Directly from Eq. (9), the discretized transport equation for h and Ω are:

$$h^{n+1} = h^n + F(u^*, \Delta t; h^\theta) + G(v^*, \Delta t; h^\lambda) \tag{14}$$

$$\Omega^{n+1} = \Omega^n + F(u^*, \Delta t; \Omega^\theta) + G(v^*, \Delta t; \Omega^\lambda) \tag{15}$$

where

$$()^\theta = ()^n + \tfrac{1}{2} g[\overline{v^*}^\lambda, \Delta t; ()^n], \text{ and } ()^\lambda = ()^n + \tfrac{1}{2} f[\overline{u^*}^\lambda, \Delta t; ()^n].$$

It is stressed here that we will not actually update Ω^n to Ω^{n+1}. Instead, only the absolute vorticity fluxes will be used for the discretization of the right hand sides of Eqs. (11) and (12). The time-averaged absolute vorticity fluxes are the components that make up the discretized transport equation. This is a 'reverse-engineering' procedure: that is, given a final product we determine how to assemble that product by tearing it apart, component by component.

To complete the discretization of (11) and (12), the pressure gradient terms are discretized with the 'economical explicit' or the 'forward–backward scheme' (Mesinger and Arakawa 1976; Haltiner and Williams 1980), which is conditionally stable and second-order accurate if it is combined with a *forward-in-time* advection scheme such as the one used here. The final form of the momentum equations are

$$u^{n+1} = u^n + \Delta t \left\{ \mathcal{Y}(v^*, \Delta t; \Omega^\lambda) - \frac{1}{A \Delta\lambda \cos\theta} \delta_\lambda \left[\kappa^* + \overline{\overline{\Phi^{n+1}}^\lambda}^\theta \right] \right\} \tag{16}$$

$$v^{n+1} = v^n - \Delta t \left\{ \mathcal{X}(u^*, \Delta t; \Omega^\theta) + \frac{1}{A \Delta\theta} \delta_\theta \left[\kappa^* + \overline{\overline{\Phi^{n+1}}^\lambda}^\theta \right] \right\} \tag{17}$$

where κ, the upstream-biased 'kinetic energy' defined at the four corners of the cell (the hollow circles in Fig. 2), is formulated as

$$\kappa^* = \tfrac{1}{2} \left\{ \mathcal{X}(\overline{u^*}^\theta, \Delta t; u^n) + \mathcal{Y}(\overline{v^*}^\lambda, \Delta t; v^n) \right\}. \tag{18}$$

The above form of κ minimizes the inconsistency in the momentum equation and thus avoids the 'Hollingsworth–Kållberg instability'. It can be readily verified that (15) can be recovered by taking 'curl' of the two components, (16) and (17), of the vector momentum equation provided the *cell-averaged* relative vorticity is computed by the Stokes theorem as follows:

$$\nabla \times \mathbf{V}^n = \frac{1}{A^2 \Delta\lambda \Delta\theta \cos\theta} \int_c \mathbf{V}^n \cdot \mathbf{dl}$$

$$= \frac{1}{A \Delta\lambda \cos\theta} \delta_\lambda v^n - \frac{1}{A \Delta\theta \cos\theta} \delta_\theta [u^n \cos\theta] \tag{19}$$

where the contour integral is taken counter-clockwise along the boundary of a cell and $\mathbf{dl}$ represents an element of the contour. At the two poles, the relative vorticity is similarly

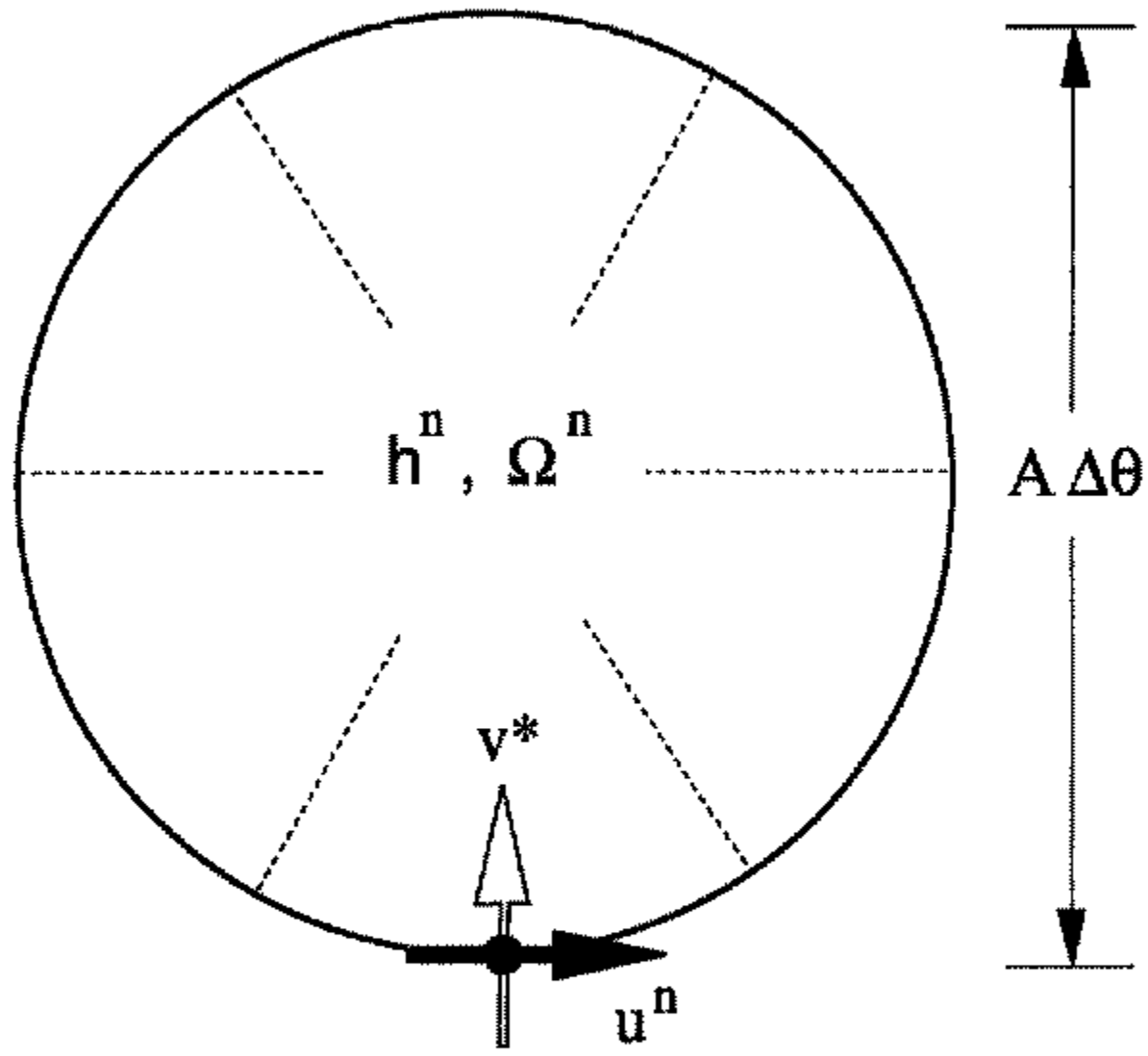

Figure 3. Schematics of the North polar cap. The *great circle distance* from one side of the polar cap to the opposite side is $A\Delta\theta$. The edge of the polar cap is located at $\theta = \frac{\pi}{2} - \frac{\Delta\theta}{2}$.

computed as the net circulation around the 'polar cap' divided by the total area of the polar cap, which is equal to $2\pi A^2[1 - \cos(\Delta\theta/2)]$. The polar cap is defined as the cell enclosing the pole (see Fig. 3; see also Lin *et al.* 1994 for details of determining the fluxes into or out of the polar cap).

Insofar we have not addressed how the time-centred winds $\mathbf{V}^* = (u^*, v^*)$ on the C-grid are obtained. A simple way to accomplish this is by a second-order extrapolation in time followed by an averaging process in space (from the D-grid to the C-grid).

$$\mathbf{V}^* = \overline{\overline{\tfrac{3}{2}\mathbf{V}^n - \tfrac{1}{2}\mathbf{V}^{n-1}}^{\lambda}}^{\theta} \tag{20}$$

This time extrapolation technique has been widely used in 'two-time-level' semi-implicit semi-Lagrangian models (e.g., Temperton and Staniforth 1987; see also the review by Staniforth and Côté 1991). Unfortunately, in addition to being more memory intensive (two time levels of winds must be saved), simulations using (14), (16) and (17) with the advective winds computed by (20) contain some mild two-grid-length gravity-wave oscillations when sharp bottom topography is present. To eliminate this problem, we discard the time extrapolation procedure and advance the advective winds at time-level n on the C-grid (obtained by spatial averaging) for a half time-step to obtain the desired time-centred values. We are, in effect, employing a two-grid two-step time marching procedure. As in AL's method, the vorticity on the C-grid is defined at the four cell corners (the hollow circles in Fig. 2), not the centre of the cell (the mass point) as on the D-grid. Unlike AL's method, this does not corrupt the functional relation between h and Ω because C-grid variables h^* and (u^*, v^*) are not prognostic variables in this C–D-grid algorithm. They are discarded after the prognostic variables h^n and (u^n, v^n), which are defined on the D-grid, are updated for one time-step.

For clarity, we describe next the complete cycle of the time marching. Assuming the time integration starts from time-level n, before updating the prognostic variables on the D-grid for a full time-step to time-level $n + 1$, the time-centred advective winds (u^*, v^*)

on the C-grid are computed as follows (cf, Eqs. (14), (16) and (17)).

$$h^* = h^n + F\left(u_c^n, \frac{\Delta t}{2}; h^{\theta/2}\right) + G\left(v_c^n, \frac{\Delta t}{2}; h^{\lambda/2}\right) \tag{21}$$

$$u^* = u_c^n + \frac{\Delta t}{2}\left\{\mathcal{Y}\left(v^n, \frac{\Delta t}{2}; \Omega_c^{\lambda/2}\right) - \frac{1}{A\Delta\lambda\cos\theta}\delta_\lambda[\kappa^{**} + \Phi^*]\right\}, \tag{22}$$

$$v^* = v_c^n - \frac{\Delta t}{2}\left\{\mathcal{X}\left(u^n, \frac{\Delta t}{2}, \Omega_c^{\theta/2}\right) + \frac{1}{A\Delta\theta}\delta_\theta[\kappa^{**} + \Phi^*]\right\}, \tag{23}$$

where

$$h^{\lambda/2} = h^n + \frac{1}{2}f\left(u_a^n, \frac{\Delta t}{2}; h^n\right), \quad h^{\theta/2} = h^n + \frac{1}{2}g\left(v_a^n, \frac{\Delta t}{2}, h^n\right),$$

$$\Omega_c^{\lambda/2} = \Omega_c^n + \frac{1}{2}f\left(u_b^n, \frac{\Delta t}{2}, \Omega_c^n\right), \quad \Omega_c^{\theta/2} = \Omega_c^n + \frac{1}{2}g\left(v_b^n, \frac{\Delta t}{2}, \Omega_c^n\right),$$

$$u_b^n = \overline{u^n}^\lambda,\ v_b^n = \overline{v^n}^\theta,$$

$$u_c^n = \overline{u_b^n}^\theta,\ v_c^n = \overline{v_b^n}^\lambda,$$

$$u_a^n = \overline{u_c^n}^\lambda,\ v_a^n = \overline{v_c^n}^\theta,$$

$$\Omega_c^n = 2\omega\sin\theta + \nabla\times\mathbf{V}_c^n,$$

and κ^{**}, the upwind-biased kinetic energy defined at the mass point, is computed as

$$\kappa^{**} = \frac{1}{2}\left[\mathcal{X}\left(u_a^n, \frac{\Delta t}{2}; u_c^n\right) + \mathcal{Y}\left(v_a^n, \frac{\Delta t}{2}; v_c^n\right)\right]. \tag{24}$$

After (u^*, v^*) are obtained, prognostic variables h^n and (u^n, v^n) are updated using Eqs. (14), (16) and (17) which completes a time marching cycle.

Obtaining the advective winds using Eqs. (21), (22) and (23) is more expensive than simply using Eq. (20). However, the extra CPU time is well spent because the two-grid-length waves are eliminated without resorting to additional and often *ad hoc* damping mechanisms. In this two-grid system, the divergence of the advective winds (u^*, v^*) and the 'curl' of the prognostic winds (u^n, v^n), the relative vorticity, are defined at the same 'mass point'. As observed by Randall (1994), with the Z-grid the components of the divergent part of the wind 'want' to be staggered as in the C-grid, while the components of the rotational part of the wind 'want' to be staggered as in the D-grid. Therefore, as far as the linear behavior of the system is concerned, our two-grid system is essentially the same as the Z-grid. Due to the use of the 'reversed-engineering approach' there is no need to invert the vorticity and divergence, which is a great computational advantage. This two-grid system is similar to the time and space staggered 'CC' or 'DD'-grid discussed by Fox–Rabinovitz (1991). However, aside from the fact that we are not using centre (in time and/or in space) differencing techniques, our two-grid system is self advancing and no previous or current information on the C-grid is needed or used. (The time-centred advective winds on the C-grid are computed from the current D-grid variables.) Using the terminology of Fox–Rabinovitz, we shall term our two-grid system the CD-grid.

The algorithm developed above can be easily applied to a regional model if appropriate boundary conditions are supplied. There is formally no time-step restriction associated with the advective processes. There is, however, a stability condition imposed by the gravity-wave processes, which are treated explicitly (see Mesinger and Arakawa 1976 for the stability analysis of the forward-backward scheme). For our intended application on the

whole sphere, a polar filter is therefore recommended for computational efficiency. The purpose of the polar filter is to stabilize the short-in-length (and high-in-frequency) gravity waves that are being unnecessarily and unidirectionally resolved at very high latitudes in the zonal direction. To minimize distortion to the meteorologically more important larger-scale waves, the polar Fourier filter is very scale selective and is only applied to the tendency term in the h^* Eq. (21), to u^* and v^*, and to the tendency terms in (16) and (17). The strength of the Fourier filter is similar to the one described by Suarez and Takacs (1995) for a C-grid model using a fourth-order extension of Arakawa and Lamb's centre differencing method. Because our prognostic variables are computed on the D-grid, and the fact that the FFSL transport scheme is stable for Courant number greater than one, in nonlinear cases in which the transport–advection processes are important the maximum size of the time-step is about two to three times larger than a model based on Arakawa and Lamb's method. This is verified in the shallow-water system and in 3-D dynamical cores for the GEOS-GCM (Suarez and Takacs 1995).

For the sake of generality, we have not specified the 1-D scheme to be used for the (inner) advective-form operators (f and g) and the (outer) flux-flux operators (F and G). It is found by numerical experiments that using lower-order operators in computing the advective winds has no significant effects on the overall accuracy. In the numerical examples to be presented in the next section, we used the unconstrained second-order van Leer scheme for the computation of all the fluxes associated with the computation of the advective winds (Eqs. (21), (22) and (23)) on the C-grid and the more accurate (but more CPU time demanding) monotonicity-preserving PPM for updating the prognostic variables on the D-grid. The first order upwind scheme is always used for inner advective-form operators (see LR) on both grids. This strategy saves about 25 to 40% of the total CPU time without noticeable impact on the quality of the simulations.

4. Computational examples

The algorithm developed in the previous section has been extensively tested using various initial conditions, including analyzed wind and height fields, with or without bottom topography. Idealized experiments include tests with north–south symmetry (to test that the model can maintain symmetry), extreme gradients, and balanced steady-state flows. These tests were useful in guiding the details in the design of the algorithm. For instance, the time extrapolation technique for obtaining the 'time-centred' advective winds on the C-grid (Eq. (20)) was discarded after it is discovered that short-wavelength noises were generated in the height field (h) in the presence of sharp bottom topography.

Williamson *et al.* (1992, W92 hereafter) proposed several test cases for comparing numerical algorithms for solving shallow-water equations on the sphere. We will present two selected cases here. (Test case 1, the pure advection case, was presented in Lin and Rood (1996) in which a convergence test of the FFSL scheme was also given.) In addition, we will also present a case in which an initially zonally symmetric flow was forced by a time-dependent wavenumber-1 'mountain' to emulate the Rossby wave-breaking event in the stratosphere [see Juckes and McIntyre 1987; Norton 1994; and Bates and Li 1996 (B96)]. Unless otherwise specified, all computations were done on the CRAY C-90 with 64-bit floating point precision.

The first case selected for presentation is the 'Test Case 5' from W92, which examines the nonlinear evolution of a zonal flow impinging on an isolated mountain (see W92 for details). We will not perform direct error analysis against the published reference resolution obtained with a T213 spectral model (see Jakob *et al.* 1993 (J93) and Jakob *et al.* 1995 (J95)). We will, instead, perform the test with three different resolutions

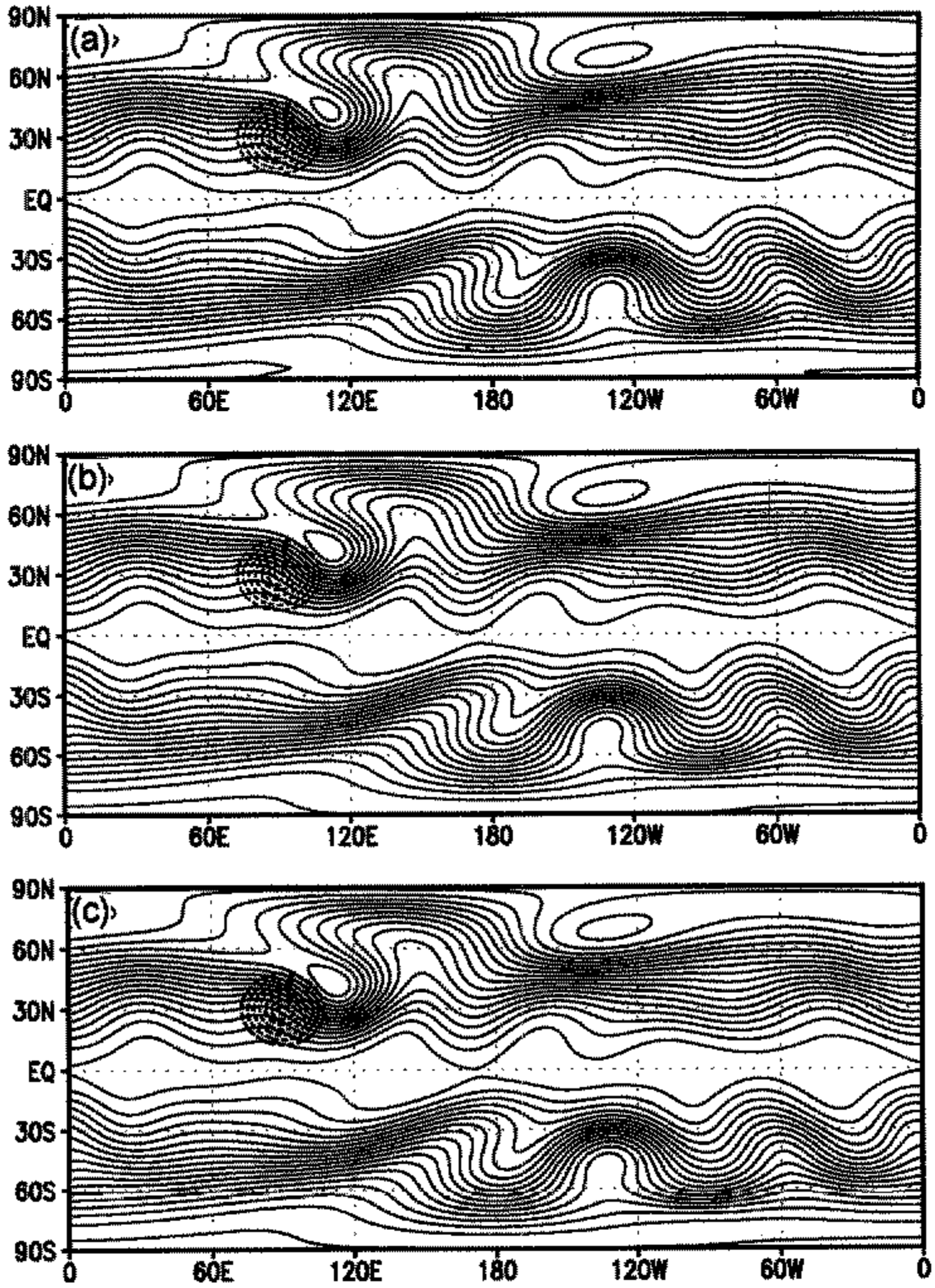

Figure 4. Height fields at DAY-15 for the test case 5 from Williamson *et al.* (1992) for the 128 × 64–600 model (a), the 256 × 128–300 model (b), and the 512 × 256–150 model (c). Contour interval: 50 m. Orography contours are dashed.

to examine the convergence of the solutions. The resolution is denoted as $M \times N - \Delta t$, where $M = 2\pi/\Delta\lambda$, $N = \pi/\Delta\theta$, and Δt, if present, indicates the size of the time-step in seconds. The model therefore has $M \times (N - 1)$ grid cells plus two polar caps. To match, as close as possible, the spectral method's resolution (on the Gaussian grid), the chosen resolutions are $128 \times 64 - 600$, $256 \times 128 - 300$, and $512 \times 256 - 150$. The 128×64 spatial resolution has nearly the same total number of grid points as the Gaussian grid in a T42 spectral model, which is a resolution typically used in long-term climate simulations. The 512×256 resolution has nearly the same amount of grid points as the Gaussian grid in the T170 spectral model, a resolution closer to that of a medium-range numerical weather prediction model. Figures 4, 5, and 6 show at DAY-15 the total height field (h plus the height of the mountain), zonal wind u, and meridional wind v at these three resolutions. The winds were averaged to the mass point for the graphical presentation.

The solutions at three different resolutions are almost identical, indicating that, for this particular problem, convergence has been nearly achieved at these resolutions. They are

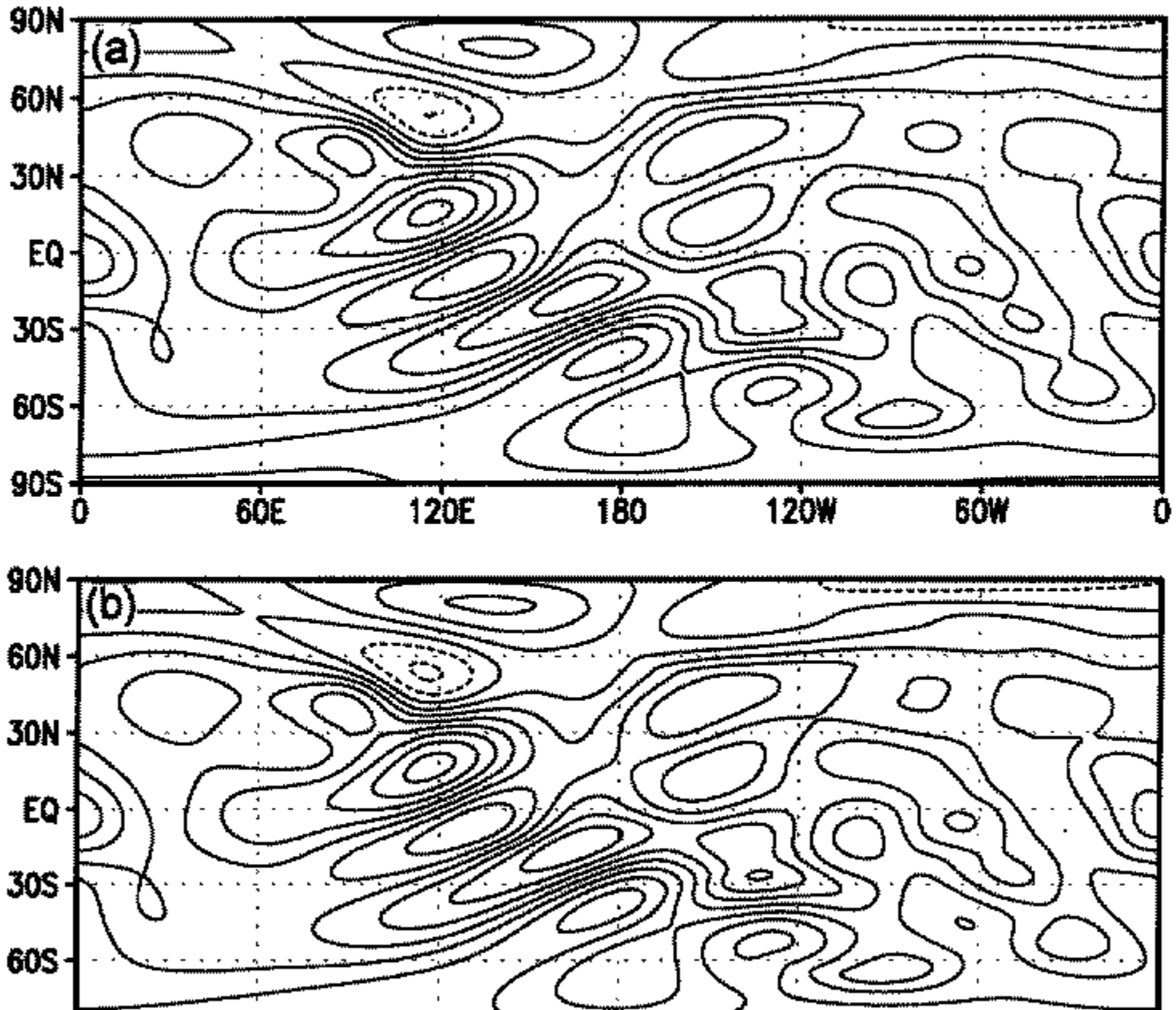

Figure 5. As in Fig. 4, but for the zonal wind (u) field. Contour interval: 5 m s^{-1}. Negative contours are dashed.

all free of the small-scale oscillations generated upstream of the mountain in the spectral solutions (including the T213 reference solution) of J95. There is also more structure in the tropics of the spectral model solutions. Referring to Fig. 4, it is difficult to find any differences in the height field at the three different resolutions. The zonal and meridional wind fields (Figs. 5 and 6) exhibit small differences in the extrema of the fields. All large-scale features of the height fields are nearly the same as the T213 reference solution (Fig. 5.1 in J95) except in the tropics and on the upstream side of the mountain where the T213 solution exhibits mild oscillations and more small-scale structure. This may be due to 'Gibb's oscillations' in the spectral solution to problem.

The second test case is 'Test Case 6' (see W92 for details), a wavenumber-4 Rossby–Haurwitz wave initial condition. The wavenumber-4 Rossby–Haurwitz wave is empirically known to be a stable solution to the shallow-water equations. A question posed in J95 is 'how long the initial solution should be expected to be stable'. Based on a 60-day integration with the T42 model (with a 600-second time-step), J95 (see also, W92) concluded that

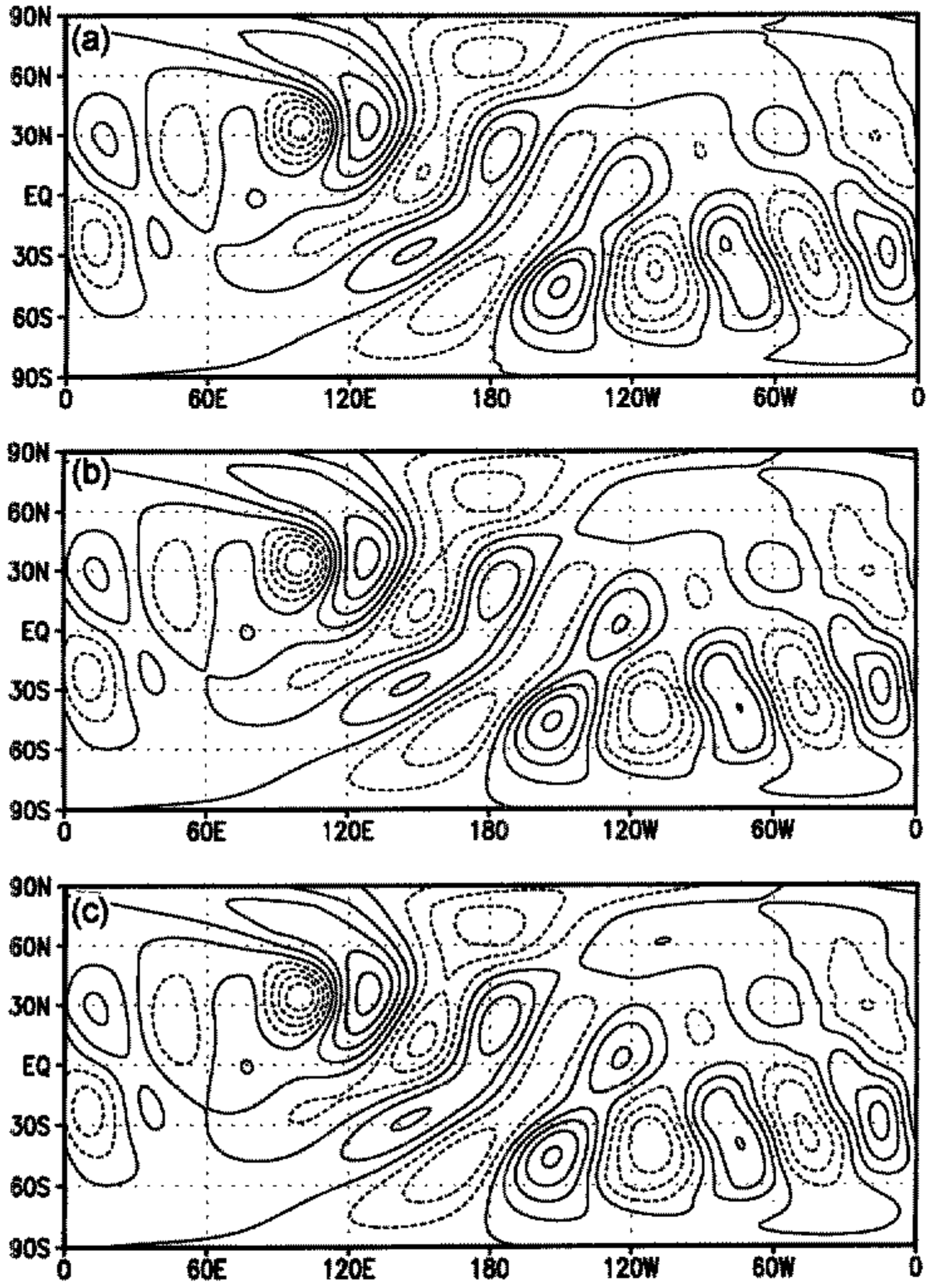

Figure 6. As in Fig. 4, but for the meridional wind (v) field. Contour interval: 5 m s^{-1}. Negative contours are dashed.

viable numerical methods should be able to maintain the basic wavenumber-4 structure for a minimum 14-day time-span.

We integrated our low-resolution $128 \times 64 - 600$ model, comparable to T42, also for 60 days. The initial condition is computed directly from the analytic form using point-wise values, not cell-averaged value. Figure 7 shows the percentage changes in the total energy and potential enstrophy as a function of time. After an initial adjustment period the rates of decay decrease and approach constant rates after about 10 days. Figure 8 shows the solutions at DAY-14, DAY-30, and DAY-60. The solution at DAY-14 is remarkably similar to that of the T42 spectral model (Fig. 5.7 in J95), both in phase and in amplitude. However, the solutions at DAY-30 and DAY-60 are clearly less deformed than those of the T42 (see Fig. 6.11 in Jakob *et al.* 1993). Smolarkiewicz and Margolin (1993) also performed this test using the same spatial resolution (but with a much smaller 40-second time-step). Their solutions (see their Fig. 2) appear to be more damped than the spectral solution and the one presented here.

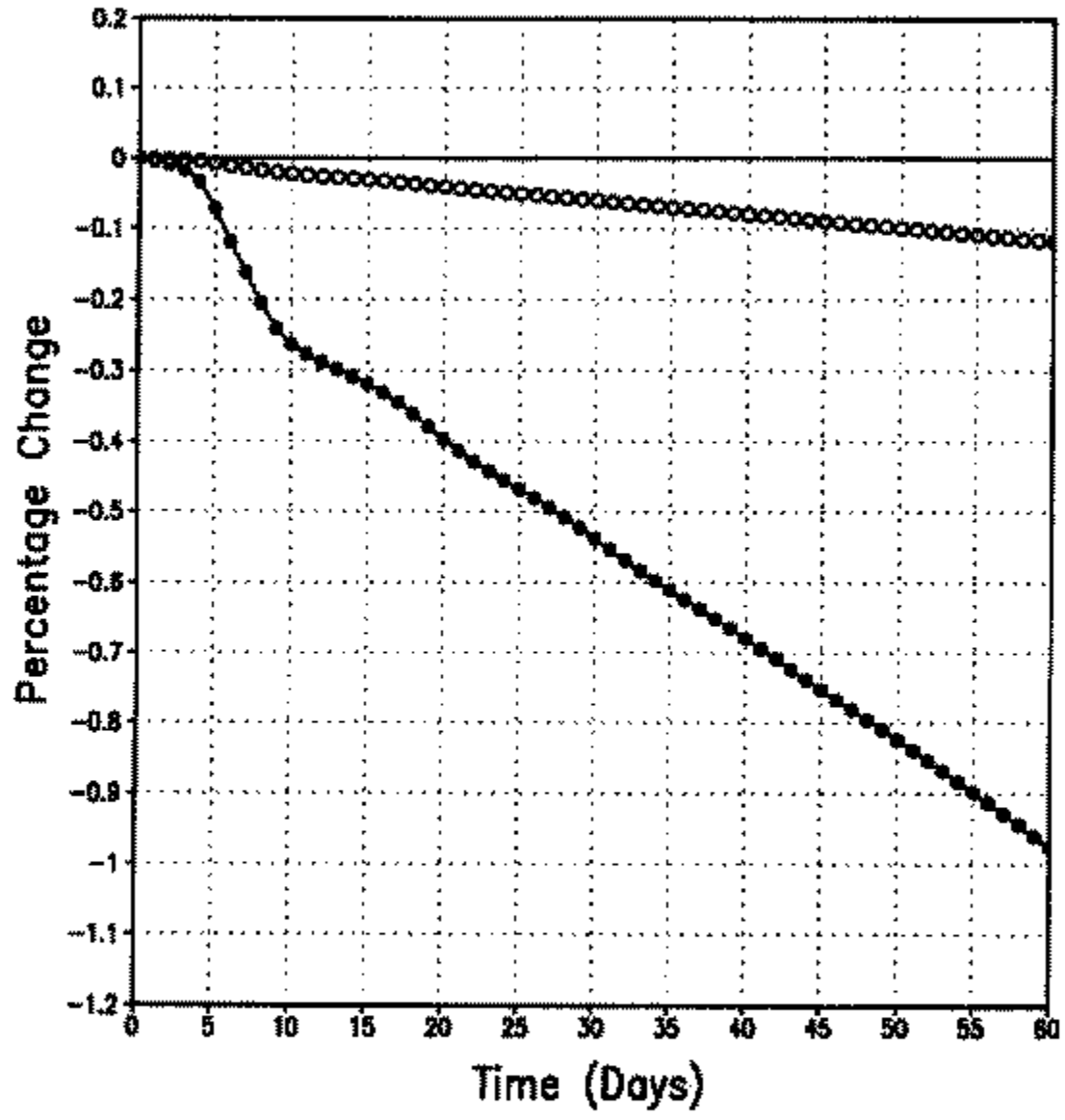

Figure 7. Percentage changes in the total mass (the solid line), total energy (the hollow circles), and potential enstrophy (the solid circles) as functions of time for the wavenumber-4 Rossby–Haurwitz test case. The total mass is conserved to machine precision.

As there is no known exact solution, no absolute conclusions can be made regarding the accuracy of a particular algorithm. The spectral transform method has a unique advantage for this test case because the initial flow field can be exactly represented by the basis functions which are spherical harmonics. In addition, the spectral method, like the Arakawa–Lamb's centre differencing method, is non-dissipative, which is best suited for preserving long wave structures such as the wavenumber-4 structure in this test case. In contrast, this test case is quite a challenge to models based on a dissipative transport algorithm like the one presented here, or the one presented by Smolarkiewicz and Margolin (1993) based on the MPDATA scheme (Smolarkiewicz 1984). The test results suggest that the implicit diffusion associated with the 2-D FFSL scheme (based on the 1-D PPM operator) is not as strong as the explicit scale selective ∇^4 diffusion in the spectral model (with the diffusion coefficient recommended in J93) or the implicit diffusion in the MPDATA scheme.

Several factors can affect the distortion of the height fields as the approximate solution evolves in this Rossby–Haurwitz test case. Besides the advection scheme, the basic formulation of the model (e.g., the way variables are staggered) can impact the solution. However, it is our conjecture that the deformation of the wave-4 structure is mainly caused by the diffusion whether implicit or explicit, or alternatively whether of a numerical or physical character. To investigate this further, the experiment was repeated but with the 1-D PPM operator replaced by the more dissipative second-order van Leer operator (using the monotonicity constraint given by Eq. 5 in Lin *et al.* 1994). (Note that the PPM is formally fourth-order accurate in 1-D for smooth flows.) The solutions thus obtained are shown in Fig. 9. A stable wavenumber-4 structure is still maintained at DAY-60, but the solutions appear to be more deformed than the T42 spectral solutions. Nonetheless, the phase is still nearly the same as the PPM solution and the T42 spectral solution, which is a very encouraging agreement. This suggests that the scale-dependent diffusion implicit

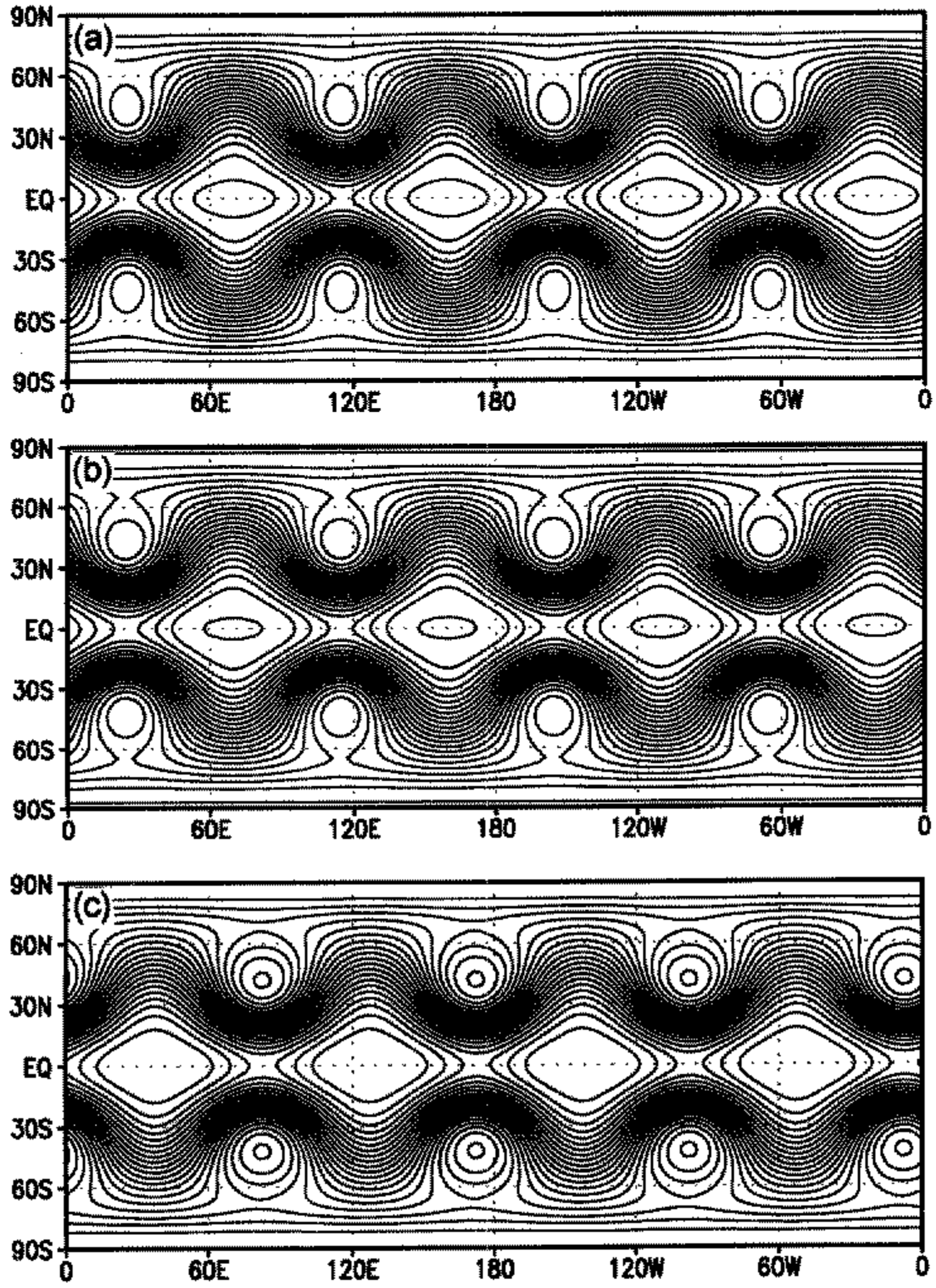

Figure 8. Height fields at DAY-14 (a), DAY-30 (b), and DAY-60 (c) for the wavenumber-4 Rossby–Haurwitz test case using the 128 × 64–600 model with PPM as the 1-D flux-form operator. Contour interval is 100 m.

in the 1-D operators (van Leer or PPM) does not adversely impact the phase speed of the waves.

We also tested the model on a SUN workstation using only 32-bit precision. The much larger rounding errors caused the model to develop some initially small but asymmetric perturbations that after approximately 50 days grew to corrupt the wavenumber-4 structure. Repeating the run on the SUN with 64-bit arithmetic eliminated this problem.

The final case to be presented is the simulation of 'stratospheric vortex erosion' first studied by Juckes and McIntyre (1987) using a non-divergent barotropic model. Originally this experiment was pursued to develop underlying theories of stratospheric dynamics, and the consequences of dynamical isolation on the distribution of trace species. However, it is also an interesting and very challenging case to examine numerics.

Numerous studies using shallow-water models as well as contour dynamics have been carried out to investigate the vortex erosion problem (e.g., Norton 1994; Waugh 1993; B96, and references therein). B96 investigated three different numerical approximations

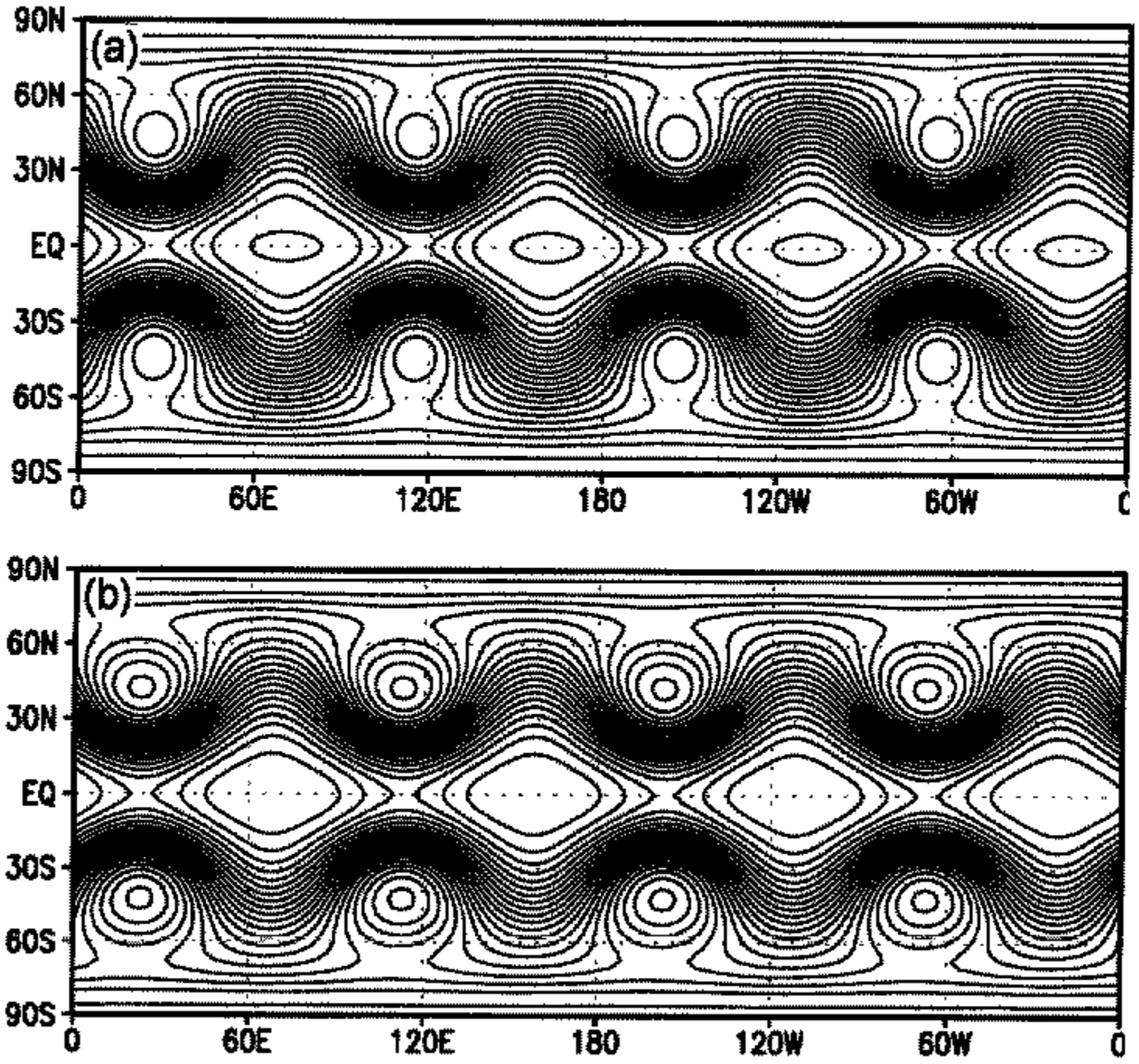

Figure 9. As in Fig. 8, but the PPM operator was replaced by the monotonic van Leer operator.

to the shallow-water equations. We follow the same configuration as B96 to facilitate comparisons.

In the configuration used in B96 and here (see B96 for details), an initially circular polar vortex is forced 'from below' by a time-dependent wavenumber-1 'mountain'. Through nonlinear interaction, smaller-and-smaller-scale structures gradually develop, as visualized by the evolution of the potential vorticity (PV) contours. A damping mechanism, implicit or explicit, is therefore needed to provide an energy and enstrophy cascade to the unresolvable scales. A stable vortex core, formation of the strong PV gradients (PV filaments), clear signature of the Rossby wave breaking, and the formation of the mid-latitude surf zone are the important features of this problem. As in the first example, we performed this simulation with three different resolutions. Due to the nature of this problem, the convergence of the solution is more difficult to achieve. This test case is far more challenging than the previous two standard test cases.

Figure 10 shows the PV contours of these three runs at DAY-24 (using the same contour interval as in B96). There are larger differences than in the 'Test Case 5' shown

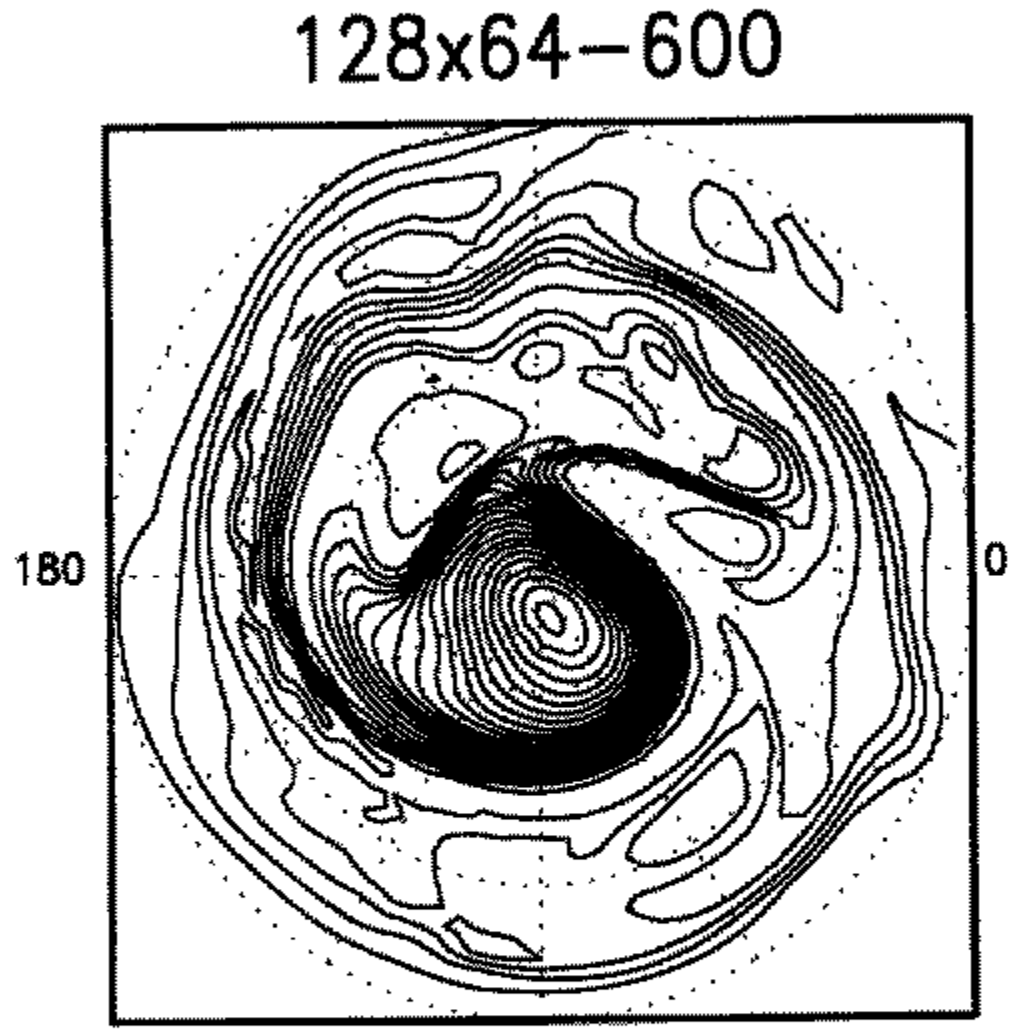

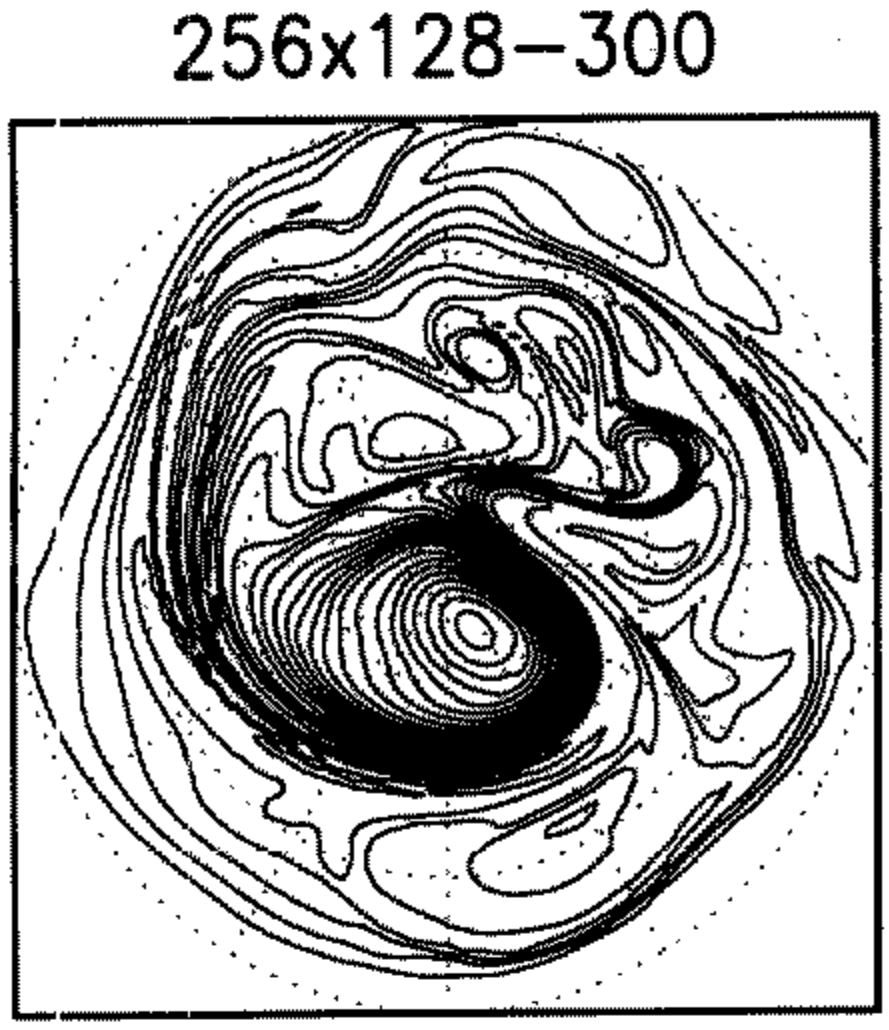

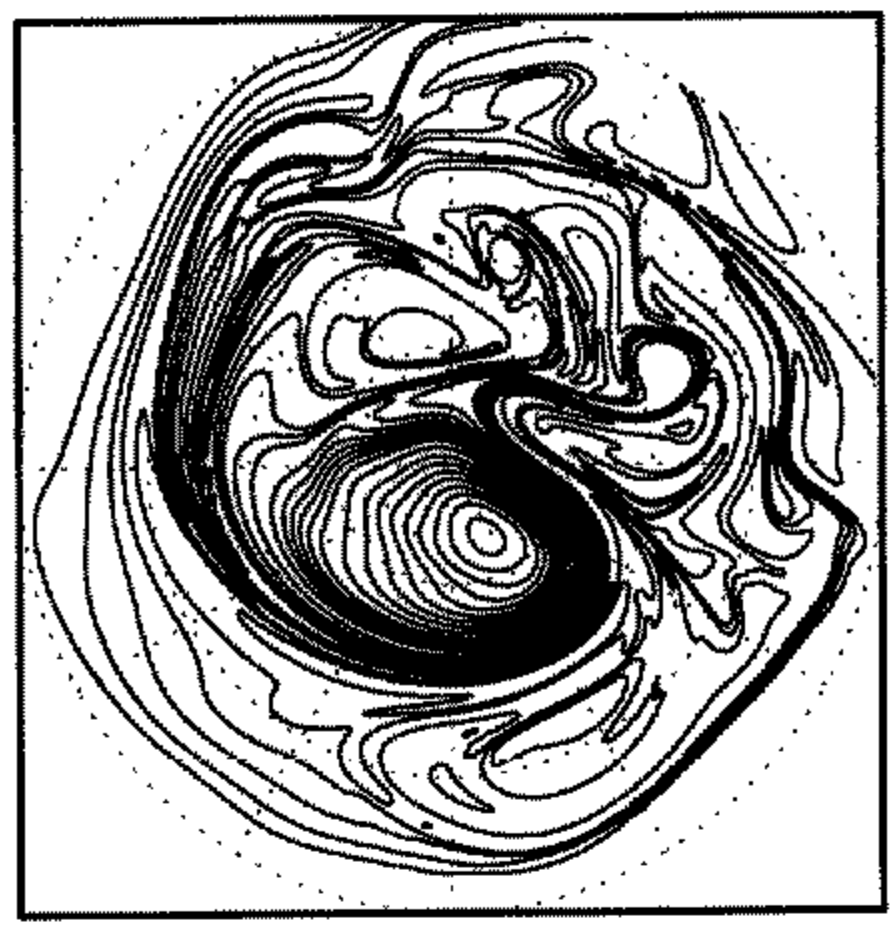

Figure 10. Polar stereographic projection (from the equator to the north pole) of the potential vorticity contours at DAY-24 in the 'stratospheric vortex erosion' test case at three different resolutions.

in Figs. 4 to 6. The 128 × 64 resolution misses many features visible in the two higher resolution runs. This is especially obvious in longitudes 120° to 180° and latitudes 30° to 60°. Also a blocky character is evident in the line of strong PV gradient that extends from longitudes 10°–160° and latitudes 30°–60°. This blocky nature is characteristic of monotonicity algorithms that are not well matched to their application (see Rood 1987). In the 256 × 128 experiment the blocky structure has moved down the spatial scale and is visible in the 270°–360° quadrant. In the 128 × 64 experiment this quadrant is significantly more diffused. The PV gradients are very sharp in the 256 × 128 and the 512 × 256 runs. The 512 × 256 run, in particular, developed sharp separation between polar and midlatitude 'air' reminiscent of the results from contour dynamics and contour advection studies.

B96 presented results with two semi-implicit semi-Lagrangian models, one based on the momentum equation (the u–v semi-Lagrangian model; hereafter, u–v SLM) and the other based on the potential vorticity–divergent formulation (PV–D model, see B95 for

details). Both models are non-conservative. The results obtained by the spectral model (Hack and Jakob 1992) are also presented in B96. While our model and the PV–D model have essentially no adjustable parameters, the spectral model, as noted in B96, must use a diffusion coefficient 10 times larger than the 'recommended value' (see Table 3 in J93) to prevent a noisy solution. With the exception of u–v SLM, the solutions from the different models agree reasonably well with the results shown here. The model described here gives the sharpest gradients at all three resolutions.

Takacs (1995, personal communication) also carried out the same test using a model based on a fourth-order extension of Arakawa–Lamb's method, which is used in the GEOS model (Suarez and Takacs 1995). The solutions from the u–v SLM and the GEOS dynamical core fall into the same family, and show some distinct differences from the ones shown here and those obtained by the PV–D and the spectral models. The most notable differences are in the tongue of vortex air being drawn towards middle latitudes in the 0°–90° longitude quadrant. The differences may be related to the fact that u–v SLM and the model based on Arakawa–Lamb's method maintain less well the functional relation between h and Ω. This is because the two conservative variables are treated inconsistently by different numerical algorithms. The potential vorticity, which is often regarded as a dynamical tracer, is a simple function of Ω and h (i.e., PV $= \Omega/h$). The PV–D model trivially enforced the relation because PV itself is a prognostic variable. The spectral model, like the model described here, also has no such problem because h and Ω are treated in a consistent manner.

5. Concluding remarks

A novel method for the discretization of the shallow-water equations on the sphere using regular latitude–longitude coordinates is described. Mass (the depth of fluid) and absolute vorticity are transported conservatively and consistently by the multidimensional FFSL scheme (Lin and Rood 1996), which is based on 1-D monotonicity-preserving finite-volume schemes such as the PPM. Gravity waves are treated consistently by the explicit 'forward–backward' approach of Mesinger and Arakawa (1976) in a two-grid system, which we termed the 'CD grid'. This two-grid system has the advantage of the Z-grid (Randall 1994), but without the need to invert vorticity and divergence.

Three test cases have been presented, and the results were compared with published results from models based on fundamentally different algorithms. The FFSL algorithm is shown to be very competitive in accuracy for a given resolution. Compared with the spectral method, the FFSL algorithm is free of high wavenumber distortion near mountainous regions. The basic wave-4 structure in the Rossby–Haurwitz wave test case is maintained much better than the spectral model in long-term integration. More diffusive versions of the FFSL algorithm do show similarities to the spectral solutions. As there is no externally adjustable parameter, the monotonicity constraint associated with the 1-D finite-volume flux-form operators acts like a 'smart' subgrid-scale flux parametrization, which is nonlinear and adaptive to flow situations. This is particularly evident in the stratospheric vortex erosion case. While this implicit subgrid mixing-diffusion has some expected characteristics of physical mixing, further study is required to characterize the reality of the subgrid mixing processes.

The algorithm is self advancing (i.e., no information from the previous time-step is needed). Therefore, the core memory usage is about half of that required by the two-time-level semi-Lagrangian models or the spectral models based on the leapfrog time differencing scheme. The total CPU time required per time-step with the 128×64 model using PPM as the 1-D operators is about 0.017 seconds on a single processor C-90, which is about three times faster than that of the semi-implicit semi-Lagrangian PV–D model

(B95). The computational efficiency depends on the size of the chosen time-step. Because gravity waves are treated explicitly, the maximum allowable time-step is much smaller than that of a semi-implicit semi-Lagrangian model whose time-step is limited by accuracy consideration alone. Therefore, our explicit algorithm may not be overall as fast, in terms of total CPU time, as the more traditional semi-implicit semi-Lagrangian methods on a vector processing computer (the C-90). However, aside from the fact that it is conservative, our algorithm appears to offer better accuracy at a given resolution in the cases we studied. In addition, since there is no need to solve an elliptic equation, which is a global problem, a fully explicit algorithm is expected to perform relatively better on the Massively Parallel Platforms. If this turns out not to be the case, a semi-implicit treatment of the gravity-wave processes can be implemented. Machenhauer and Olk (1995) have successfully implemented a semi-implicit algorithm with a 'cell-integrated semi-Lagrangian' (CISL) scheme. The CISL scheme is fundamentally equivalent to the FFSL scheme in the 1-D setting of Machenhauer and Olk. However, it would be more desirable to solve the vorticity–divergence form (in 2D) in the semi-implicit formulation, instead of the current two-grid two-step procedure.

The FFSL algorithm can be readily extended to 3-D hydrostatic primitive equations and applied to general circulation models. The explicit algorithm is currently being implemented in a dynamical core for the GEOS–GCM. Preliminary tests indicated that it is about as fast as the operational dynamical core using a fourth-order extension of the Arakawa–Lamb method (with a rotated pole) on the CRAY C-90 and J-90.

References

Allen, D. J., Douglass, A. R., Rood, R. B. and Guthrie, P. D. 1991 Application of a monotonic upstream-biased transport scheme to three-dimensional constituent transport calculations. *Mon. Weather Rev.*, **119**, 2456–2464

Arakawa, A. 1966 Computational design for long-term numerical integration of the equations of fluid motions: Two-dimensional incompressible flow. Part I. *J. Comp. Phys.*, **1**, 119–143

Arakawa, A. and Lamb, V. R. 1981 A potential enstrophy and energy conserving scheme for the shallow-water equations. *Mon. Weather Rev.*, **109**, 18–36

Bates, J. R., Moorthi, S. and Higgins, R. W. 1993 A global multilevel atmospheric model using a vector semi-Lagrangian finite-difference scheme. Part I: Adiabatic formulation. *Mon. Weather Rev.*, **121**, 244–263

Bates, J. R., Li, Y., Brandt, A., McCormick, S. F. and Ruge, J. 1995 A global shallow-water numerical model based on the semi-Lagrangian advection of potential vorticity. *Q. J. R. Meteorol. Soc.*, **121**, 1981–2005

Bates, J. R. and Li, Y. 1996 Simulation of stratospheric vortex erosion using three different global shallow water numerical models. In *Numerical methods for atmospheric and ocean modelling*. André. J. Robert memorial volume of *Atmos.–Ocean*

Bourke, W. 1972 An efficient, one-level, primitive equation spectral model. *Mon. Weather Rev.*, **100**, 683–689

Carpenter, Jr., R. L., Drogemeier, K. K., Woodward, P. R. and Hane, C. E. 1990 Application of the piecewise parabolic method to meteorological modelling. *Mon. Weather Rev.*, **118**, 586–612

Colella, P. and Woodward, P. R. 1984 The piecewise parabolic method (PPM) for gas-dynamical simulations. *J. Comp. Phys.*, **54**, 174–201

Fox-Rabinovitz, M. S. 1991 Computational dispersion properties of horizontal staggered grids for atmospheric and ocean models. *Mon. Weather Rev.*, **119**, 1624–1639

Haltiner, G. J. and Williams, R. T. 1980 *Numerical prediction and dynamic meteorology*. John Wiley, New York

Hack, J. J. and Jakob, R. 1992 'Description of global shallow-water model based on the spectral transform method.' NCAR Technical Note, NCAR/TN–343+STR

Harten, A. 1983 High resolution schemes for conservation laws. *J. Comp. Phys.*, **49,** 357–393

Hollingsworth, A., Kållberg, P., Renner, V. and Burridge, D. M. 1983 An internal symmetric computational instability. *Q. J. R. Meteorol. Soc.*, **109,** 417–428

Jakob, R., Hack, J. J. and Williamson, D. L. 1993 'Solutions to the shallow-water test set using the spectral transform method.' NCAR Technical Note, NCAR/TN 388+STR

Juckes, M. N. and McIntyre, M. E. 1987 A high-resolution one-layer model of breaking planetary waves in the stratosphere. *Nature*, **328,** 590–596

Lin, S.-J., Chao, W. C., Sud, Y. C. and Walker, G. K. 1994 A class of the van Leer-type transport schemes and its applications to the moisture transport in a general circulation model. *Mon. Weather Rev.*, **122,** 1575–1593

Lin, S.-J. and Rood, R. B. 1996 Multidimensional flux-form semi-Lagrangian transport schemes. *Mon. Weather Rev.*, **124,** 2046–2070

Machenhauer, B. and Olk, M. 1995 'The implementation of the semi-implicit scheme in cell-integrated semi-Lagrangian models.' Max-Planck-Institute for Meteorology, Report No. **156**

Mesinger, F. and Arakawa, A. 1976 'Numerical methods used in atmospheric models.' GARP Publications Series No. 17, WMO-ICSU Joint Organizing Committee, World Meteorological Organization, Geneva

Norton, W. 1994 Breaking Rossby waves in a model stratosphere diagnosed by a vortex-following coordinate system and a technique for advecting material contours. *J. Atmos. Sci.*, **51,** 654–673

Randall, D. A. 1994 Geostrophic adjustment and the finite-difference shallow-water equations. *Mon. Weather Rev.*, **122,** 1371–1377

Rasch, P. J. and Williamson, D. L. 1991 The sensitivity of a general circulation model climate to the moisture transport formulation. *J. Geophys. Res.*, **96,** 13, 123–137

Ritchie, H., Temperton, C., Simmons, A., Hortal, M., Davies, T., Dent, D. and Hamrud, M. 1995 Implementation of the semi-Lagrangian method in a high-resolution version of the ECMWF forecast model. *Mon. Weather Rev.*, **123,** 489–514

Rood, R. 1987 Numerical advection algorithms and their role in atmospheric transport and chemistry models. *Rev. Geophys.*, **25,** 71–100

Rood, R. B., Nielsen, J. E., Stolarski, R. S., Douglass, A. R., Kaye, J. A. and Allen, D. J. 1992 Episodic total ozone minima and associated effects on heterogeneous chemistry and lower stratospheric transport. *J. Geophys. Res.*, **96,** 5055–5071

Sadourny, R. 1975 The dynamics of finite difference methods of the shallow-water equations. *J. Atmos. Sci.*, **32,** 680–689

Shapiro, R. 1970 Smoothing, filtering and boundary effects. *Rev. Geophys. Space Phys.*, **8,** 359–387

Smagorinsky, J., Manabe, S. and Holloway, J. L. 1965 Numerical results from a nine-level general circulation model of the atmosphere. *Mon. Weather Rev.*, **93,** 727–768

Smolarkiewicz, P. K. 1982 The multi-dimensional Crowley advection scheme. *Mon. Weather Rev.*, **110,** 1968–1983

1984 A fully multidimensional positive definite advection transport algorithm with small implicit diffusion. *J. Comp. Phys.*, **54,** 325–362

Smolarkiewicz, P. K. and Margolin, L. G. 1993 On forward-in-time differencing for fluids: extension to a curvilinear framework. *Mon. Weather Rev.*, **121,** 1847–1859

Staniforth, A. and Côté, J. 1991 Semi-Lagrangian integration schemes for atmospheric models—A review. *Mon. Weather Rev.*, **119,** 2206–2223

Suarez, M. J. and Takacs, L. L. 1995 'Documentation of the ARIES/GEOS dynamical core: Version 2.' NASA Technical Memorandum 104606, Vol. **5**

Tanguay, M., Robert, A. and Laprise, R. 1990 A semi-implicit semi-Lagrangian fully compressible regional forecast model. *Mon. Weather Rev.*, **118,** 1970–1980

Temperton, C. and Staniforth, A. 1987 An efficient two-time-level semi-Lagrangian semi-implicit integration scheme. *Q. J. R. Meteorol. Soc.*, **113,** 1025–1039

Thuburn, J. 1993 Use of a flux-limited scheme for vertical advection in a GCM. *Q. J. R. Meteorol. Soc.*, **119,** 469–487

Van Leer, B. 1974 Toward the ultimate conservative difference scheme. II: Monotonicity and conservation combined in a second order scheme. *J. Comp. Phys.*, **14,** 361–370

1977 Toward the ultimate conservative difference scheme. IV: A new approach to numerical convection. *J. Comp. Phys.*, **23,** 276–299

Van Leer, B. 1979 Toward the ultimate conservative difference scheme. V: A second order sequel to Godunov's method. *J. Comp. Phys.*, **32,** 101–136

Waugh, D. W. 1993 Contour surgery simulations of a forced polar vortex. *J. Atmos. Sci.*, **50,** 714–730

Williamson, D. L. and Rasch, P. J. 1989 Two-dimensional semi-Lagrangian transport with shape preserving interpolation. *Mon. Weather Rev.*, **117,** 102–129

Williamson, D. L., Drake, J. B., Hack, J. J., Jakob, R. and Swarztrauber, P. N. 1992 A standard test set for numerical approximations to the shallow-water equations in spherical geometry. *J. Comp. Phys.*, **102,** 211–224

Williamson, D. L. and Olson, J. G. 1994 Climate simulations with a semi-Lagrangian version of the NCAR CCM2. *Mon. Weather Rev.*, **122,** 1594–1610

Woodward, P. R. and Colella, P. 1984 The numerical simulation of two-dimensional fluid flow with strong shocks. *J. Comp. Phys.*, **54,** 115–173

Zalesak, S. T. 1979 Fully multidimensional flux-corrected transport algorithms for fluid. *J. Comp. Phys.*, **31,** 335–362